Contemporary Mathematics
https://ojs.wiserpub.com/index.php/CM/

Research Article

Efficient Spectral Collocation Schemes for Nonlinear ψ-Caputo Fractional Riccati Differential Equations with Variable-Order

A. Emin[1], M. A. Abdelkawy[2], Anjan Biswas[3,4,5*]

[1] Department of Software Engineering, Istanbul Gelisim University, Istanbul 34310, Turkey
[2] Department of Mathematics and Statistics, College of Science, Imam Mohammad Ibn Saud Islamic University (IMSIU), Riyadh 11432, Saudi Arabia
[3] Department of Mathematics and Physics, Grambling State University, Grambling, LA 71245-2715, USA
[4] Department of Physics and Electronics, Khazar University, Baku AZ-1096, Azerbaijan
[5] Department of Mathematics and Applied Mathematics, Sefako Makgatho Health Sciences University, Pretoria 0204, South Africa
E-mail: biswasa@gram.edu

Received: 30 June 2025; **Revised:** 10 October 2025; **Accepted:** 6 November 2025

Abstract: This article presents a spectral method for estimating solutions of the nonlinear Variable-Order Caputo ψ-Fractional Riccati Differential Equation (VOC-ψ-FRDE). First, the solution and its ψ-fractional derivatives are expressed using a series of Shifted Legendre Polynomials (SLPs). Then, the expansion coefficients are determined by transforming the VOC-ψ-FRDE along with its associated conditions into an algebraic system. The effectiveness and feasibility of the proposed approach are demonstrated through various numerical tests.

***Keywords*:** Caputo ψ fractional of variable order, Spectral collocation method, Fractional Riccati Differential Equation (FRDE), Shifted Legendre Polynomials (SLPs)

MSC: 65M70, 34K37, 42C10

1. Introduction

Fractional Differential Equations (FDEs) [1–3] have wide applications across various fields due to their ability to simulate complex memory-related phenomena, hereditary properties, and non-local effects. One prominent application of FDEs is in physics [4, 5], where they are used to characterize the behavior of materials with time-dependent properties, such as creep and relaxation. In engineering, FDEs are employed in control theory to design controllers for systems with fractional-order dynamics [6], enhancing performance and stability. Additionally, they play a crucial role in modeling biological processes [7], including population dynamics, cell growth, and drug transport in tissues, where fractional calculus effectively captures non-local and memory effects for accurate predictions and analysis. Furthermore, FDEs find applications in finance for modeling complex market behaviors [8] and in signal processing for analyzing signals with long-term dependencies and non-local correlations [9].

Fractional Riccati Differential Equations (FRDEs) play a significant role in physics due to their ability to model complex systems with memory and hereditary properties, which are often described using fractional calculus. These equations extend the classical Riccati differential equations by incorporating fractional derivatives, allowing for a more

DOI: https://doi.org/10.37256/cm.7320267646

accurate representation of phenomena such as anomalous diffusion, viscoelasticity, and non-Markovian processes. In physics, FRDEs are particularly useful in quantum mechanics, where they describe systems with fractional dynamics, and in statistical mechanics, where they model non equilibrium processes. Additionally, FRDEs find applications in control theory, signal processing, and the study of nonlinear waves in plasmas and optics. The fractional nature of these equations provides a powerful tool for understanding systems with long-range interactions and time-dependent behaviors that cannot be adequately described by integer-order differential equations. Rabiei and Razzaghi [10] introduced fractional Boubaker wavelets to solve FRDEs. Similarly, Yuttanan [11] proposed fractional-order generalized Legendre wavelets and applied them to solve FRDEs via the hypergeometric function. Doha et al. [12] developed a spectral method to approximate variable-order FRDEs by expanding the solution in terms of shifted Chebyshev polynomial series. Momani [13] implemented a numerical approach based on the iterative reproducing-kernel algorithm for solving FRDEs. Tvyordyj [14] studied FRDEs with a variable fractional derivative, capturing the hereditary properties of the medium and its dependence on past states. They developed a numerical scheme by employing finite differences to approximate the variable-order derivative and to solve the resulting nonlinear algebraic system. The authors in [15] presented an efficient and stable local Radial Basis Function (RBF) partition of unity method to numerically solve the time-fractional Black-Scholes equation, while in [16] the authors proposed an accurate and robust two-step algorithm combining Crank-Nicolson time discretization with nonuniform meshes, Galerkin finite element spatial discretization, and an Alternating Direction Implicit (ADI) scheme to efficiently solve the 3D nonlocal heat equation with a weakly singular kernel. In [17] the authors developed and analyzed efficient Backward Euler (BE)- and Second-Order Backward Differentiation Formula (BDF2)-based finite difference schemes for the generalized tempered integro-differential equation.

Variable-Distributed Order Fractional Riccati Differential Equations (VDO-FRDEs) constitute a fascinating and complex area of mathematical modeling. These equations extend classical Riccati equations by incorporating fractional derivatives of variable order and distributed memory effects. This enables them to describe a broader range of phenomena where both the order of differentiation and the system's memory vary. Analyzing VDO-FDEs with ψ are particularly challenging, as traditional methods for solving Riccati equations often fail due to the variable order and distributed nature of the fractional derivative.

In [18], the author utilized a ψ-Haar wavelet operational matrix to solve ψ Riccati fractional differential equations, whereas [19] presents several theorems related to the ψ variable order. In [20], the authors solved ψ-Caputo time-fractional systems by applying the Laplace transform, fixed-point theory, and Grönwall's inequality. Similarly, [21] introduced the ψ-Caputo fractional derivative approach for solving fractional partial differential equations using the ψ-Haar wavelet operational matrix. Furthermore, Zhao et al. [22] applied the mapped Jacobi function and the Petrov-Galerkin spectral method to ψ-fractional differential equations involving boundary and initial conditions.

The proposed method has promising applications in control and synchronization of nonlinear systems. In adaptive fuzzy control [23], it can yield more accurate reference trajectories, while in output-feedback projective lag-synchronization [24], it enhances modeling of variable-order dynamics under uncertainty. When combined with robust neural adaptive control [25], it provides precise state estimates that improve robustness, and in adaptive backstepping control [26], it enables more effective treatment of system uncertainties. These applications highlight the method's value not only as a numerical scheme but also as a tool for advancing fractional-order control and synchronization.

For four decades, spectral methods have been widely applied across various fields, as highlighted in [27–32]. Initially, Fourier-based spectral methods were restricted to specific cases, such as periodic boundary conditions and simple geometries. However, recent theoretical advancements have significantly expanded their applicability, enabling effective solutions to a wide range of problems. Compared to other numerical methods, spectral approaches offer superior accuracy and exponential convergence rates. These methods represent solutions as finite series of orthogonal functions. Several spectral techniques exist, including collocation [33–36], tau [37–40], Galerkin [41, 42], and Petrov-Galerkin [2, 43, 44], where coefficients are optimized to minimize absolute errors. For instance, spectral collocation approximates differential equation solutions with remarkable accuracy, allowing residuals to approach zero at specific points.

When implementing the Shifted Legendre Polynomial (SLP) spectral collocation, the choice of collocation nodes strongly influences how rapidly the discrete solution error decreases with polynomial degree. If the exact solution (in the ψ-transformed variable) is analytic on an open region containing the physical interval, interpolation by shifted Legendre

polynomials at appropriately chosen nodes yields (near-)exponential convergence as the polynomial degree increases. In practice the two common node families are Shifted Legendre-Gauss (SL-G) and Shifted Legendre-Gauss-Lobatto (SL-GL) points. SL-GL nodes include the interval endpoints and therefore allow direct enforcement of boundary/initial conditions and typically simplify construction of differentiation matrices used in collocation; they also cluster near endpoints which helps to resolve boundary-layer behaviour or endpoint singularities that frequently appear in fractional problems. SL-G nodes (which exclude endpoints) often provide slightly better interior approximation and more accurate quadrature for inner products but require special treatment to impose endpoint conditions.

For variable-order ψ-fractional problems, endpoint regularity is decisive: if the solution displays reduced smoothness at an endpoint, it clustering of SL-GL nodes improves local resolution and prevents severe degradation of the convergence rate. Conversely, if the solution is globally analytic in the ψ-domain, both SL-G and SL-GL collocation recover spectral decay of the error; differences are then primarily practical. Finally, node choice also interacts with nonlinear terms: denser sampling near regions where nonlinearities vary rapidly reduces aliasing error and improves the effective convergence. In our experiments (Section 4) we therefore use SL-GL nodes as a robust default and report the observed exponential decay for smooth test solutions; we also demonstrate how reduced endpoint regularity slows convergence unless endpoint clustering or a weighted basis is used. This approach employs fractional SL-GL points to approximate solutions for nonlinear Variable-Order Caputo ψ-Fractional Riccati Differential Equations (VOC-ψ-FRDEs). The VOC-ψ FRDEs are expressed as a series of fractional SLPs using the fractional differential operator ψ. The residuals of these equations are evaluated at the SL-GL quadrature points, resulting in a system of algebraic equations that is then solved. Numerical experiments are conducted to validate the effectiveness of this methodology.

The principal contributions of this work can be summarized as follows.

(i) We propose, for the first time, a spectral scheme based on Shifted Legendre Polynomials (SLPs) for solving the nonlinear Variable-Order Caputo ψ-Fractional Riccati Differential Equation (VOC-ψ-FRDE).

(ii) The method efficiently transforms the VOC-ψ-FRDE, together with its associated conditions, into an algebraic system that is straightforward to implement numerically.

(iii) The approach fully exploits the orthogonality and approximation power of SLPs, leading to high-accuracy results with relatively low computational cost.

(iv) The effectiveness and feasibility of the proposed approach are validated through a set of numerical experiments, which demonstrate its robustness and superiority compared to existing techniques. These features collectively underscore the originality and practical relevance of the present study.

This paper is structured as follows: Section 2 introduces the fundamental concepts of ψ fractional calculus and reviews the key properties of SLPs. Section 3 discusses the spectral collocation method for solving nonlinear VOC-ψ-FRDEs. Section 4 presents numerical examples to demonstrate the efficacy and accuracy of the proposed methodology. Finally, Section 5 summarizes the findings and provides conclusions based on the results.

2. Fundamental concepts

2.1 *The ψ fractional calculus*

This section outlines essential concepts, definitions, and results from ψ-fractional calculus that will be utilized in the following sections. For $p \geq 1$, the space $L_p^{\psi}(c, d)$, denotes the set of Lebesgue measurable functions on the finite interval (c, d) that are p-integrable with respect to the measure $d\psi$:

$$L_{\psi}^{p}(c, d) := \left[\mathscr{Y}: \int_c^d |\hat{\mathscr{U}}(\chi)|^p d\psi < \infty\right],$$

$L_{\psi}^{p}(c, d)$ is a Banach space with norm $\|\mathscr{Y}\|_{L_{\psi}^{p}}$,

$$\|\mathscr{Y}\|_{L_\psi^p} = \left(\int_c^d |(\hat{\chi})|^p d\psi \right)^{1/p}.$$

When $p = 2$, space $L_\psi^p(c, d)$ transforms into a Hilbert space with inner product:

$$(\mathscr{Y}, \hat{\mathscr{V}})_\psi = \int_c^d \mathscr{Y}(\chi)\hat{\mathscr{V}}(\chi)d\psi.$$

We utilize $L_\psi^2(c, d)$ for weighted Hilbert space with inner product:

$$(\mathscr{Y}, \hat{\mathscr{V}})_\Omega = \int_c^d \mathscr{Y}(\chi)\hat{\mathscr{V}}(\chi)\Omega(\chi)d\chi.$$

Definition 1 [7, 45] The left- and right-sided ψ-fractional integrals of a function $\hat{\mathscr{U}}(\chi)$ with order $\alpha_1 > 0$ are defined as

$${}_\psi D_{c,\chi}^{-\alpha_1} = \frac{1}{\Gamma(\alpha_1)} \int_c^\chi \psi'(\rho)\big(\psi(\chi) - \psi(\rho)\big)\big)^{\alpha_1 - 1} \hat{\mathscr{U}}(\rho)d\rho, \quad \chi \in (c, d),$$

$${}_\psi D_{\chi,d}^{-\alpha_1} = \frac{1}{\Gamma(\alpha_1)} \int_\chi^d \psi'(\rho)\big(\psi(\rho) - \psi(\chi)\big)\big)^{\alpha_1 - 1} \hat{\mathscr{U}}(\rho)d\rho, \quad \chi \in (c, d).$$

In the preceding formulation, the condition $\hat{\mathscr{U}}(\chi) \in L_\psi^1(c, d)$ is frequently assumed to be necessary but applicable. The options of ψ in the preceding definition are as follows.

Remark 1 Definition 1 defines fractional operators ${}_\psi D_{c,\chi}^{-\alpha_1}$ and ${}_\psi D_{\chi,d}^{-\alpha_1}$, which generalize existing fractional integral operators:

- $\psi(\chi) = \chi$ is the classical Riemann-Liouville-type fractional integral.
- $\psi(\chi) = log(\chi)$ is the Hadamard fractional integral [46–48].
- $\psi(\chi) = exp(\chi)$ is the fractional integral with exponential kernel [49].

Lemma 1 [45] The semigroup property described below is applicable: for $\alpha_1, \beta_1 > 0$

$${}_\psi D_{c,\chi}^{-\alpha_1}({}_\psi D_{c,\chi}^{-\beta_1}\hat{\mathscr{U}}(\chi)) = {}_\psi D_{c,\chi}^{-(\alpha_1+\beta_1)}\hat{\mathscr{U}}(\chi), \qquad {}_\psi D_{\chi,d}^{-\alpha_1}({}_\psi D_{\chi,d}^{-\beta_1}\hat{\mathscr{U}}(\chi)) = {}_\psi D_{\chi,d}^{-(\alpha_1+\beta_1)}\hat{\mathscr{U}}(\chi).$$

Lemma 2 [7, 50] The findings below are applicable for $\alpha_1 > 0$, $\beta_1 > -1$

$${}_\psi D_{c,\chi}^{-\alpha_1}\big(\psi(\chi) - \psi(c)\big)^\nu = \frac{\Gamma(\nu+1)}{\Gamma(\nu+\alpha_1+1)}\big(\psi(\chi) - \psi(c)\big)^{\nu+\alpha_1},$$

$${}_\psi D_{\chi,d}^{-\alpha_1}\big(\psi(d) - \psi(\chi)\big)^\nu = \frac{\Gamma(\nu+1)}{\Gamma(\nu+\alpha_1+1)}\big(\psi(d) - \psi(\chi)\big)^{\mu+\alpha_1}.$$

Definition 2 [45] For $\chi \in (c, d)$, the left- and right-sided ψ-Riemann-Liouville fractional derivatives (also known as ψ-derivatives) of a given function $\hat{\mathscr{U}}(\chi)$ with order $\alpha_1 > 0$ are defined as

$$ {}_{\psi}D_{c,\chi}^{-\alpha_1}\hat{\mathscr{U}}(\chi) = \delta_{\psi}^{n}\left[{}_{\psi}D_{c,\chi}^{-(n-\alpha_1)}\hat{\mathscr{U}}(\chi)\right] = \frac{1}{\Gamma(n-\alpha_1)}\delta_{\psi}^{n}\int_{c}^{\chi}\psi'(\rho)\big(\psi(\chi)-\psi(\rho)\big)^{n-\alpha_1-1}\hat{\mathscr{U}}(\rho)d\rho, $$

$$ {}_{\psi}D_{\chi,d}^{-\alpha_1}\hat{\mathscr{U}}(\chi) = (-1)^{n}\delta_{\psi}^{n}\left[{}_{\psi}D_{\chi,d}^{-(n-\alpha_1)}\hat{\mathscr{U}}(\chi)\right] = \frac{(-1)^{n})}{\Gamma(n-\alpha_1)}\delta_{\psi}^{n}\int_{\chi}^{d}\psi'(\rho)\big(\psi(\rho)-\psi(\chi)\big)^{n-\alpha_1-1}\hat{\mathscr{U}}(\rho)d\rho. $$

Definition 3 [45] For $\chi \in (c, d)$, the left-sided and right-sided ψ-Caputo fractional derivatives of a known function $\hat{\mathscr{U}}(\chi)$ with order$\alpha_1 \in (n-1, n)$, $n \in N+$ are defined as:

$$ {}_{C}\psi D_{c,\chi}^{\alpha_1}\hat{\mathscr{U}}(\chi) = {}_{\psi}D_{c,\chi}^{-(n-\alpha_1)}\left[\delta_{\psi}^{n}\hat{\mathscr{U}}(\chi)\right] = \frac{1}{\Gamma(n-\alpha_1)}\int_{c}^{\chi}\psi'(\rho)\big(\psi(\chi)-\psi(\rho)\big)^{n-\alpha_1-1}\delta_{\psi}^{n}\hat{\mathscr{U}}(\rho)d\rho, $$

$$ {}_{C}\psi D_{\chi,d}^{\alpha_1}\hat{\mathscr{U}}(\chi) = (-1)^{n}{}_{\psi}D_{\chi,d}^{-(n-\alpha_1)}\left[\delta_{\psi}^{n}\hat{\mathscr{U}}(\chi)\right] = \frac{(-1)^{n}}{\Gamma(n-\alpha_1)}\int_{\chi}^{d}\psi'(\rho)\big(\psi(\rho)-\psi(\chi)\big)^{n-\alpha_1-1}\delta_{\psi}^{n}\hat{\mathscr{U}}(\rho)d\rho. $$

Definition 4 [19, 51] The left fractional integral of a function $\hat{\mathscr{U}}$ of order $\alpha_1(\chi)$ with regard to the kernel ψ is described below:

$$ I_{c+}^{\alpha_1(\chi)}\hat{\mathscr{U}}(\chi) = \frac{1}{\Gamma(\alpha_1(\chi))}\int_{c}^{\chi}\psi'\big(\psi(\chi)-\psi(\rho)\big)^{\alpha_1-1}\hat{\mathscr{U}}(\rho)d\rho. $$

However, the right fractional integral is determined as

$$ I_{d-}^{\alpha_1(\chi)}\hat{\mathscr{U}}(\chi) = \frac{1}{\Gamma(\alpha_1(\chi))}\int_{\chi}^{d}\psi'\big(\psi(\rho)-\psi(\chi)\big)^{\alpha_1-1}\hat{\mathscr{U}}(\rho)d\rho. $$

Definition 5 [19, 51] We describe two distinct types of Riemann-Liouville fractional derivatives: type 1 and type 2. The left Riemann-Liouville fractional derivative type 1 of function $\hat{\mathscr{U}}$ (order α_1, kernel ψ) is defined as:

$$ {}_{1}D_{c+}^{\alpha_1}\hat{\mathscr{U}}(\chi) = \frac{1}{\Gamma(1-\alpha_1(\chi))}\Big(\frac{1}{\psi'(\chi)}\frac{d}{d\chi}\Big)\int_{c}^{\chi}\psi'\big(\psi(\chi)-\psi(\rho)\big)^{-\alpha_1(\chi)}\hat{\mathscr{U}}(\rho)d\rho. $$

The right one can be described as:

$$ {}_{1}D_{d-}^{\alpha_1}\hat{\mathscr{U}}(\chi) = \frac{1}{\Gamma(1-\alpha_1(\chi))}\Big(\frac{-1}{\psi'(\chi)}\frac{d}{d\chi}\Big)\int_{c}^{\chi}\psi'\big(\psi(\rho)-\psi(\chi)\big)^{-\alpha_1(\chi)}\hat{\mathscr{U}}(\rho)d\rho. $$

The left and right operators for the Riemann-Liouville fractional derivative type 2 are as follows:

$$ {}_2D_{c+}^{\alpha_1}\hat{\mathscr{U}}(\chi)=\Big(\frac{1}{\psi'(\chi)}\frac{d}{d\chi}\Big)\Big[\frac{1}{\Gamma(1-\alpha_1(\chi))}\int_c^{\chi}\psi'\big(\psi(\chi)-\psi(\rho)\big)^{-\alpha_1(\chi)}\hat{\mathscr{U}}(\rho)d\rho\Big], $$

and

$$ {}_2D_{d-}^{\alpha_1}\hat{\mathscr{U}}(\chi)=\Big(\frac{-1}{\psi'(\chi)}\frac{d}{d\chi}\Big)\Big[\frac{1}{\Gamma(1-\alpha_1(\chi))}\int_c^{\chi}\psi'\big(\psi(\rho)-\psi(\chi)\big)^{-\alpha_1(\chi)}\hat{\mathscr{U}}(\rho)d\rho\Big]. $$

Definition 6 [19, 51, 52] The left-sided and right-sided ψ-Caputo fractional derivatives of a known function $\hat{\mathscr{U}}(\chi)$ with order $\alpha_1(\chi)$ are described as:

$$ {}^{C}{}_{\psi}D_{c+}^{\alpha_1(\chi)}\hat{\mathscr{U}}(\chi)=\frac{1}{\Gamma(1-\alpha_1(\chi))}\int_c^{\chi}\psi'(\rho)\big(\psi(\chi)-\psi(\rho)\big)^{-\alpha_1(\chi)}\frac{d}{d\rho}(\hat{\mathscr{U}}(\rho))d\rho, $$

$$ {}^{C}{}_{\psi}D_{d-}^{\alpha_{-1}(\chi)}\hat{\mathscr{U}}(\chi)=\frac{1}{\Gamma(1-\alpha_1(\chi))}\int_c^{\chi}\psi'(\rho)\big(\psi(\rho)-\psi(\chi)\big)^{-\alpha_1(\chi)}\frac{d}{d\rho}(\hat{\mathscr{U}}(\rho))d\rho. $$

Lemma 3 [50, 45] For $\hat{\mathscr{U}}\in C[c,d]$ and $\alpha_1>0$, there hold

$$ {}_{\psi}D_{c,\chi}^{\alpha_1(\chi)}({}_{\psi}D_{c,\chi}^{-\alpha_1(\chi)}\hat{\mathscr{U}}(\chi))=\hat{\mathscr{U}}(\chi),\qquad {}_{\psi}D_{\chi,d}^{\alpha_1(\chi)}({}_{\psi}D_{\chi,d}^{-\alpha_1(\chi)}\hat{\mathscr{U}}(\chi))=\hat{\mathscr{U}}(\chi), $$

and for $\hat{\mathscr{U}}\in AC_{\psi}^{n}[c,d]$

$$ \begin{aligned} {}_{\psi}D_{c,\chi}^{-\alpha_1(\chi)}({}_{\psi}D_{c,\chi}^{\alpha_1(\chi)}\hat{\mathscr{U}}(\chi))&=\hat{\mathscr{U}}(\chi)-\sum_{i=0}^{n-1}\frac{[{}_{\psi}D_{c,\chi}^{\alpha_1(\chi)-i-1}\hat{\mathscr{U}}](c)}{\Gamma(\alpha_1(\chi)-i)}(\psi(\chi)-\psi_c)^{\alpha_1(\chi)-i-1},\\ {}_{\psi}D_{\chi,d}^{-\alpha_1(\chi)}({}_{\psi}D_{\chi,d}^{\alpha_1(\chi)}\hat{\mathscr{U}}(\chi))&=\hat{\mathscr{U}}(\chi)-\sum_{i=0}^{n-1}\frac{[{}_{\psi}D_{\chi,d}^{\alpha_1(\chi)-i-1}\hat{\mathscr{U}}](c)}{\Gamma(\alpha_1(\chi)-i)}(\psi(d)-\psi_{\chi})^{\alpha_1(\chi)-i-1}. \end{aligned} \tag{1} $$

2.2 *SLP*

The Legendre polynomials $\ell_j(\mathscr{Y})(j=0,1\ldots)$ adheres to Rodrigues' formula [53].

$$ \ell_j(y)=\frac{(-1)^j}{2^j j!}D^j\big((1-y^2)^j\big). \tag{2} $$

Accordingly, $\ell_j^{(m)}(\mathscr{Y})$ is given by

$$\ell_j^{(m)}(\mathscr{Y}) = \sum_{i=0(i+j=even)}^{j-m} C_m(j,\, i)\ell_i(\mathscr{Y}), \tag{3}$$

where

$$C_m(j,\, i) = \frac{2^{m-1}(2i+1)\Gamma(\frac{m+j-i}{2})\Gamma(\frac{m+j+i+1}{2})}{\Gamma(m)\Gamma(\frac{2-m+j-i}{2})\Gamma(\frac{3-m+j+i}{2})}.$$

Then, we denote $(u,\, v)$ and $\|u\|$ as the inner product and norm within the space $L^2[-1,\, 1]$. Complete orthogonal system is the set of $\ell_k(t)$ in $L^2[-1,\, 1]$

$$(\ell_j(t),\, \ell_k(\mathscr{Y})) = \int_{-1}^{1} \ell_j(\mathscr{Y})\ell_k(\mathscr{Y})\, dt = h_k\delta_{jk}, \tag{4}$$

where $h_i = \frac{2}{2i+1}$ and δ_{jk} represents the Dirac delta function. Therefore for any $v \in L^2[-1,\, 1]$,

$$v(\mathscr{Y}) = \sum_{i=0}^{\infty} a_i\ell_i(\mathscr{Y}), \quad a_i = \frac{1}{h_i}\int_{-1}^{1} v(\mathscr{Y})\ell_i(\mathscr{Y})\, d\mathscr{Y}. \tag{5}$$

The SLPs, denoted as $\ell_{L,\,i}(\mathscr{Y})$, are defined over the range $[0,\, L]$ and can be generated using the subsequent recursive formulan: [53]

$$(j+1)\ell_{L,\,i+1}(\mathscr{Y}) = (2j+1)(\frac{2\mathscr{Y}}{L} - 1)\ell_{L,\,i}(\mathscr{Y}) - j\ell_{L,\,i-1}(\mathscr{Y}), \qquad i = 1,\, 2,\, \cdots. \tag{6}$$

The analytical expression for $\ell_{L,\,i}(\mathscr{Y})$ can be expressed as

$$\ell_{L,\,i}(\mathscr{Y}) = \sum_{j=0}^{i} (-1)^{i+j}\frac{(i+j)!}{(i-j)!\,(j!)^2 L^j}\,\mathscr{Y}^j. \tag{7}$$

The condition for orthogonality is

$$\int_0^L \ell_{L,\,i}(t)\ell_{L,\,i}(\mathscr{Y})w_L(\mathscr{Y})\, d\mathscr{Y} = h_i^L\,\delta_{ij}, \tag{8}$$

where $w_L(\mathscr{Y}) = 1$ and $h_j^L = \frac{L}{2j+1}$.

If function $\hat{\mathscr{U}}(\mathscr{Y}) \in L^2[0,\, L]$. Next, it can be represented using $\ell_{L,\,i}(\mathscr{Y})$ as

$$\hat{\mathscr{U}}(\mathscr{Y}) = \sum_{i=0}^{\infty} c_i \ell_{L,i}(\mathscr{Y}).$$

The value of c_i is determined by

$$c_i = \frac{1}{h_i^L} \int_0^L \hat{\mathscr{U}}(\mathscr{Y}) \ell_{L,i}(\mathscr{Y}) d\mathscr{Y}, \quad i = 0, 1, 2, \cdots. \tag{9}$$

Approximation $\hat{\mathscr{U}}(\mathscr{Y})$ can be expressed as:

$$\hat{\mathscr{U}}_N(\mathscr{Y}) \simeq \sum_{i=0}^{N} c_i \ell_{L,i}(\mathscr{Y}). \tag{10}$$

3. Spectral collocation for solving non-linear VOC-ψ-FRDE

This section presents a computational approach that enhances the functionality of the Shifted Legendre-Gauss-Lobatto Collocation (SL-GL-C) schemes for solving the nonlinear VOC-ψ-FRDE. Collocation points are strategically placed at the interpolation nodes of the SL-GL method. The core of our proposed algorithm involves discretizing the non-linear VOC-ψ-FRDE, resulting in a system of algebraic equations to solve for the unknown coefficients.

Specifically, we focus on the subsequent non-linear VDO-FRDEs.

$${}^{c}D_{\mathscr{Y}}^{\eta(\mathscr{Y}),\psi} \hat{\mathscr{U}}(\mathscr{Y}) + \varphi(\mathscr{Y})(\hat{\mathscr{U}}(\mathscr{Y}))^2 + \lambda(\mathscr{Y})\hat{\mathscr{U}}(\mathscr{Y}) = G(\mathscr{Y}), \quad 0 < \eta(\mathscr{Y}) < 1, \tag{11}$$

with initial condition

$$\hat{\mathscr{U}}(0) = 0, \tag{12}$$

where the functions $\eta(\mathscr{Y})$, $\lambda(\mathscr{Y})$, $\varphi(\mathscr{Y})$ are well-known, and the coefficient functions $\lambda(\mathscr{Y})$, and $\varphi(\mathscr{Y})$ are continuous and bounded, while $\hat{\mathscr{U}}(\mathscr{Y})$ is an unknown function and ${}^{C}D^{\eta(\mathscr{Y}),\psi}\hat{\mathscr{U}}(\mathscr{Y})$ represent the ψ Caputo fractional derivative of order $\eta(\mathscr{Y})$ In addition, the nonlinear operator satisfies a local Lipschitz condition in the unknown function.

Definition 7 The ψ Caputo fractional derivative [54] of order $\eta(\mathscr{Y})$ can be described as follows:

$${}^{C}D^{\eta(\mathscr{Y}),\psi}\hat{\mathscr{U}}(\mathscr{Y}) = \frac{1}{\Gamma(\gamma - \eta(\mathscr{Y}))} \int_0^{\mathscr{Y}} \psi(\varepsilon)'(\psi(\mathscr{Y}) - \psi(\varepsilon))^{\gamma - \eta(\mathscr{Y}) - 1} \hat{\mathscr{U}}^{(\gamma)}(\varepsilon) d\varepsilon, \quad \gamma - 1 < \eta(\mathscr{Y}) \leq \gamma, \ \mathscr{Y} > 0, \tag{13}$$

here, γ represents the ceiling function applied to $\eta(\mathscr{Y})$.

If $\hat{\mathscr{U}}_{Approx}(\mathscr{Y})$ is defined as an approximation of (11):

$$\hat{\mathscr{U}}_{Approx}(\mathscr{Y}) = \sum_{\tau_1 = 0, 1, \ldots, \nu_2} a_{\tau_1} \mathscr{L}_{L,\tau_1}(\mathscr{Y}), \tag{14}$$

the derivative ${}^{C}D^{\eta(\mathscr{Y}),\psi}$ of $\hat{\mathscr{U}}_{Approx}(\mathscr{Y})$ is:

$$ {}^{C}D^{\eta(\mathscr{Y}),\psi}\hat{\mathscr{U}}_{Approx}(\mathscr{Y}) = \sum_{\tau_1=0,1,\ldots,\nu_2} a_{\tau_1}^{C}D^{\eta(\mathscr{Y}),\psi}\left(\mathscr{L}_{L,\tau_1}(\mathscr{Y})\right). \tag{15} $$

By using the ψ Caputo derivative of $\eta(\mathscr{Y})$ as defined in Definition 13, we obtain:

$$ {}^{C}D^{\eta(\mathscr{Y})}\mathscr{Y}^{\tau_1} = \frac{1}{\Gamma(1-\eta(\mathscr{Y}))}\int_0^{\mathscr{Y}} \frac{\vartheta^{(\tau_1)}}{(\psi(\mathscr{Y})-\psi(\vartheta))^{\eta(\mathscr{Y})}}d\vartheta. \tag{16} $$

Therefore, it follows that:

$$ {}^{C}D^{\eta(\mathscr{Y}),\psi}\mathscr{L}_{L,\tau_1}(\mathscr{Y}) = \sum_{\tau_1=0,1,\ldots,\nu_2} (-1)^{\tau_1-\nu_2}\frac{(\nu_2+\tau_1-1)!\,2^{2\tau_1}}{(\nu_2-\tau_1)!\,(2\tau_1)!\,L^{\tau_1}}\,{}^{C}D^{\eta(\mathscr{Y}),\psi}\mathscr{Y}^{\tau_1}. \tag{17} $$

Then, we get the following:

$$ {}^{C}D^{\eta(\mathscr{Y}),\psi}\hat{\mathscr{U}}_{Approx}(\mathscr{Y}) = \sum_{\tau_1=0,1,\ldots,\nu_2} a_{\tau_1}^{C}D^{\eta(\mathscr{Y}),\psi}\left(\mathscr{L}_{L,\tau_1}(\mathscr{Y})\right) = \sum_{\tau_1=0,1,\ldots,\nu_2} a_{\tau_1}\Delta_{L,\tau_1}(\mathscr{Y}). \tag{18} $$

Equation (11) can be rewritten as:

$$ \sum_{\tau_1=0,1,\ldots,\nu_2} a_{\tau_1}\Delta_{L,\tau_1}(\mathscr{Y}) + \lambda(\mathscr{Y}) \sum_{\tau_1=0,1,\ldots,\nu_2} a_{\tau_1}\mathscr{L}_{L,\tau_1}(\mathscr{Y}) + \varphi(\mathscr{Y})\Big(\sum_{\tau_1=0,1,\ldots,\nu_2} a_{\tau_1}\mathscr{L}_{L,\tau_1}(\mathscr{Y})\Big)^2 = G(\mathscr{Y}). \tag{19} $$

The residual of Eq. (19) is set to zero by utilizing the SL-GL collocation technique at $\nu_2-1,$ of the SL-GL points. By utilizing Eq. (14)–(19), then (11) can be written as:

$$ \begin{aligned} &\sum_{\tau_1=0,1,\ldots,\nu_2} a_{\tau_1}\Delta_{L,\tau_1}(\mathscr{Y}_{L,\nu_2,i}) + \lambda(\mathscr{Y}) \sum_{\tau_1=0,1,\ldots,\nu_2} a_{\tau_1}\mathscr{L}_{L,\tau_1}(\mathscr{Y}_{L,\nu_2,i}) + \varphi(\mathscr{Y})\Big(\sum_{\tau_1=0,1,\ldots,\nu_2} a_{\tau_1}\mathscr{L}_{L,\tau_1}(\mathscr{Y}_{L,\nu_2,i})\Big)^2 \\ &= G(\mathscr{Y}_{L,\nu_2,i}). \end{aligned} \tag{20} $$

Rearranging the preceding equation results in:

$$ \begin{aligned} &\sum_{\tau_1=0,1,\ldots,\nu_2} a_{\tau_1}\left[\Delta_{L,\tau_1} + \lambda(\mathscr{Y})\mathscr{L}_{L,\tau_1}\right](\mathscr{Y}_{L,\nu_2,i}) + \varphi(\mathscr{Y})\Big(\sum_{\tau_1=0,1,\ldots,\nu_2} a_{\tau_1}\mathscr{L}_{L,\tau_1}(\mathscr{Y}_{L,\nu_2,i})\Big)^2 \\ &= G(\mathscr{Y}_{L,\nu_2,i}),\ i=1,\ldots,\nu_2. \end{aligned} \tag{21} $$

Therefore, we obtain:

$$\sum_{\tau_1=0,\,1,\,\ldots,\,\nu_2} a_{\tau_1}\Upsilon_{L,\,\tau_1}(\mathscr{Y}_{L,\,\nu_2,\,i})+\varphi(\mathscr{Y})\Big(\sum_{\tau_1=0,\,1,\,\ldots,\,\nu_2} a_{\tau_1}\mathscr{L}_{L,\,\tau_1}(\mathscr{Y}_{L,\,\nu_2,\,i})\Big)^2=G(\mathscr{Y}_{L,\,\nu_2,\,i}),\ i=1,\ldots,\nu_2, \tag{22}$$

where $\Upsilon_{L,\,\tau_1}=\left[\Delta_{L,\,\tau_1}+\lambda(\mathscr{Y})\mathscr{L}_{L,\,\tau_1}\right]$. Using Eq. (12) and (14), we acquire:

$$\sum_{\tau_1=0,\,1,\,\ldots,\,\nu_2} a_{\tau_1}\mathscr{L}_{L,\,\tau_1}(0)=0. \tag{23}$$

Equations (22), and (23) form a set of (ν_2+1) algebraic equations involving the variables $a_{\tau_1},\ \tau_1=0,\,1,\,\ldots,\,\nu_2$.

$$\begin{cases} \displaystyle\sum_{\tau_1=0,\,1,\,\ldots,\,\nu_2} (-1)^{\tau_1}a_{\tau_1}=0, \\ \\ \displaystyle\sum_{\tau_1=0,\,1,\,\ldots,\,\nu_2} a_{\tau_1}\Upsilon_{L,\,\tau_1}(\mathscr{Y}_{L,\,\nu_2,\,i})+\varphi(\mathscr{Y})\Big(\sum_{\tau_1=0,\,1,\,\ldots,\,\nu_2} a_{\tau_1}\mathscr{L}_{L,\,\tau_1}(\mathscr{Y}_{L,\,\nu_2,\,i})\Big)^2=G(\mathscr{Y}_{L,\,\nu_2,\,i}),\ i=1,\ldots,\nu_2. \end{cases} \tag{24}$$

Finally, solving the system is straightforward, allowing $\hat{\mathscr{U}}_{Approx}$ to be expressed in a closed form.

4. Numerical results

The efficiency and precision of the recommended technique are demonstrated by the following two instances; The Absolute Error (AEs) represents the discrepancy between the measured and estimated solution:

$$AEs(\mathscr{Y})=|\hat{\mathscr{U}}(\mathscr{Y})-\hat{\mathscr{U}}_{Approx}(\mathscr{Y})|, \tag{25}$$

where, at the point $\mathscr{Y}$, the approximate and exact solutions are $\hat{\mathscr{U}}(\mathscr{Y})$ and $\hat{\mathscr{U}}_{Approx}(\mathscr{Y})$. The procedure for calculating the greatest absolute errors (L_∞) and (L_2) is as outlined below:

$$L_\infty=\max\{AEs(\mathscr{Y})\}. \tag{26}$$

All numerical simulations and computations in this study were performed on a computer with an Intel Core i7 processor. The algorithm code was run via *Mathematica* version 12.2.

Example 1 Consider the non-linear VOC-ψ-FRDE:

$$\begin{cases} {}^{c}D_{\mathscr{Y}}^{\eta(\mathscr{Y}),\,\Psi}\hat{\mathscr{U}}(\mathscr{Y})+\hat{\mathscr{U}}(\mathscr{Y})+(\hat{\mathscr{U}}(\mathscr{Y}))^2=G(\mathscr{Y}), \\ \\ \mathscr{Y}(0)=0, \end{cases} \tag{27}$$

$G(\mathscr{Y})$ is given from the exact solution $\hat{\mathscr{U}}(\mathscr{Y})=(\psi(\mathscr{Y}))^2$, $\psi(\mathscr{Y})=\mathscr{Y}^3$, and $\eta(\mathscr{Y})=\mathscr{Y}\sin(\mathscr{Y}),\ \frac{1}{2}\mathscr{Y}^{\frac{1}{2}}$ where ${}^{c}D_{\mathscr{Y}}^{\eta(\mathscr{Y}),\,\Psi}\hat{\mathscr{U}}(\mathscr{Y})$ is VOC-ψ-FRDE.

We obtain AEs with various values of $\eta(\mathscr{Y})$ in Table 1, and the CPU running time is 92.688 sec. when $\eta(\mathscr{Y}) = \frac{1}{2}\mathscr{Y}^{\frac{1}{2}}$, and 138.466 when $\eta(\mathscr{Y}) = \mathscr{Y}\sin(\mathscr{Y})$. The findings indicate that the proposed method offers higher levels of accuracy. Furthermore, it is noteworthy that satisfactory approximations can be achieved using a limited number of data points. Figure 1 represents the AEs of Example 1 when $\nu_1 = 16$, $\eta(\mathscr{Y}) = \mathscr{Y}^2 cos(x)$ and $\eta(\mathscr{Y}) = \frac{\mathscr{Y}^2}{3}$ respectively. Figure 2 compare the exact and approximate solutions. When we compare Mean Absolute Error (MAE) in Table 2 between our method and the method in [18], the results show that, even by a few points, our technique is more accurate.

Table 1. The *AEs* of Example 1 with virous of $\mathscr{Y}$ and $\eta(\mathscr{Y})$ at $\nu_2 = 8$

$\mathscr{Y}$	$\nu_2 = 8$, $\eta(\mathscr{Y}) = \mathscr{Y}\sin(\mathscr{Y})$	$\nu_2 = 8$, $\eta(\mathscr{Y}) = \frac{1}{2}\mathscr{Y}^{\frac{1}{2}}$
0	2.0817×10^{-17}	3.4695×10^{-17}
0.1	2.0817×10^{-17}	3.4695×10^{-17}
0.2	2.7756×10^{-17}	3.4695×10^{-18}
0.3	1.3878×10^{-17}	2.6021×10^{-17}
0.4	1.2143×10^{-17}	8.6736×10^{-18}
0.5	3.1225×10^{-17}	0
0.6	2.7062×10^{-16}	2.2898×10^{-16}
0.7	4.7705×10^{-18}	4.5103×10^{-17}
0.8	1.1449×10^{-16}	1.5613×10^{-16}
0.9	1.4225×10^{-16}	7.9797×10^{-17}
1.0	1.6653×10^{-16}	5.5511×10^{-17}

Table 2. The *AEs* of Example 1 with virous of $\mathscr{Y}$ and $\eta(\mathscr{Y})$ at $\nu_2 = 8$

$\eta(\mathscr{Y})$	$\nu_2 = 9$, [18]	$\nu_2 = 8$, Our Method	CPU (Sec.)
0.6	4.8789×10^{-6}	1.9013×10^{-15}	26, 797
0.7	2.7562×10^{-6}	1.8804×10^{-15}	30, 75
0.8	1.5301×10^{-6}	1.7764×10^{-15}	30, 217
0.9	8.6081×10^{-7}	2.1302×10^{-15}	31, 843
1.0	5.3605×10^{-7}	1.6723×10^{-15}	18, 874

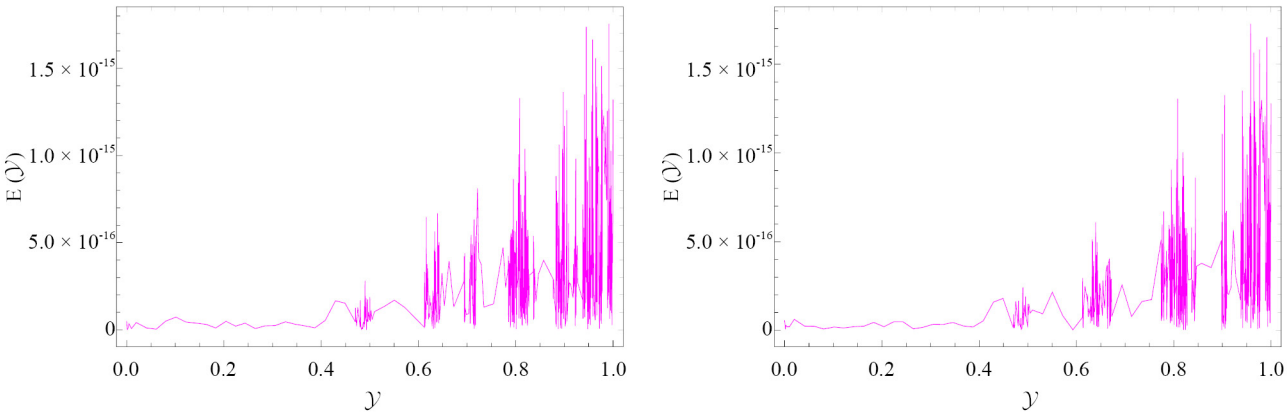

Figure 1. The AEs for Example 1 when $\nu_1 = 8$, $\eta(\mathscr{Y}) = \mathscr{Y} sin(\mathscr{Y})$ and $\eta(\mathscr{Y}) = \frac{1}{2}\mathscr{Y}^{\frac{1}{2}}$ respectively

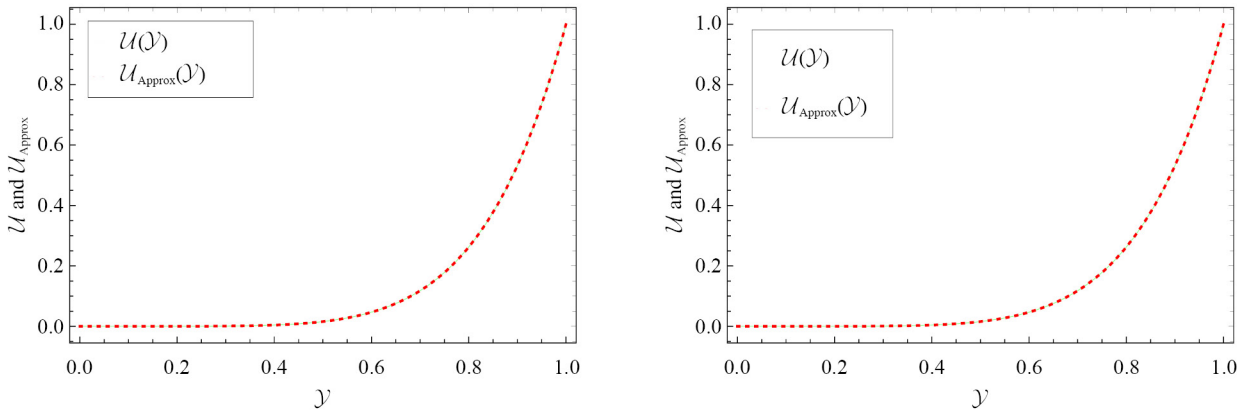

Figure 2. The $\hat{\mathscr{U}}_{Approx}(\mathscr{Y})$ and $\hat{\mathscr{U}}(\mathscr{Y})$ for Example 1 when $\nu_2 = 8$ and $\eta(\mathscr{Y}) = \mathscr{Y} sin(\mathscr{Y})$ and $\eta(\mathscr{Y}) = \frac{1}{2}\mathscr{Y}^{\frac{1}{2}}$ respectively

Taking $\nu_2 = 8$ and $\eta(\mathscr{Y}) = \mathscr{Y}^2 sin(\mathscr{Y})$, we acquire the numerical outcome $\hat{\mathscr{U}}_{Approx}(\mathscr{Y})$ of Example 1 as:

$$\begin{aligned}\hat{\mathscr{U}}_{Approx}(\mathscr{Y}) =& -1.11022\times10^{-16} - 4.44089\times10^{-16}\mathscr{Y} + 1.42109\times10^{-14}\mathscr{Y}^2 - 1.57208\times10^{-13}\mathscr{Y}^3 \\ &+ 6.53699\times10^{-13}\mathscr{Y}^4 - 1.38778\times10^{-12}\mathscr{Y}^5 + 1.\mathscr{Y}^6 - 9.26327\times10^{-13}\mathscr{Y}^7 \\ &+ 2.19253\times10^{-13}\mathscr{Y}^8.\end{aligned} \tag{28}$$

Taking $\nu_2 = 8$ and $\eta(\mathscr{Y}) = \frac{1}{2}\mathscr{Y}^{\frac{1}{2}}$, we acquire the numerical outcome $\hat{\mathscr{U}}_{Approx}(\mathscr{Y})$ of Example 1 as:

$$\begin{aligned}\hat{\mathscr{U}}_{Approx}(\mathscr{Y}) =& 0. - 9.76996\times10^{-15}\mathscr{Y}^2 + 8.61533\times10^{-14}\mathscr{Y}^3 - 3.43725\times10^{-13}\mathscr{Y}^4 + 7.39409\times10^{-13}\mathscr{Y}^5 \\ &+ 1.\mathscr{Y}^6 + 5.4344\times10^{-13}\mathscr{Y}^7 - 1.3618\times10^{-13}\mathscr{Y}^8.\end{aligned} \tag{29}$$

Example 2 Consider the non-linear VOC-ψ-FRDE:

$$\begin{cases} {}^{c}D_{\mathscr{Y}}^{\eta(\mathscr{Y}),\,\psi}\hat{\mathscr{U}}(\mathscr{Y}) + (\hat{\mathscr{U}}(\mathscr{Y}) + \hat{\mathscr{U}}(\mathscr{Y}))^3 = G(\mathscr{Y}), \\ \mathscr{Y}(0) = 0, \end{cases} \tag{30}$$

$G(\mathscr{Y})$ is given from the exact solution $\hat{\mathscr{U}}(\mathscr{Y}) = \eta(\mathscr{Y})(\psi(\mathscr{Y})^2 + 0.5\psi(\mathscr{Y}))$, $\psi(\mathscr{Y}) = \mathscr{Y}^3$, and $\eta(\mathscr{Y}) = \frac{2\mathscr{Y}}{3}$, $\frac{\mathscr{Y}^3}{3}$ where ${}^{c}D_{\mathscr{Y}}^{\eta(\mathscr{Y}),\,\psi}\hat{\mathscr{U}}(\mathscr{Y})$ is VOC-ψ-FRDE.

We obtain AEs with various values of $\eta(\mathscr{Y})$ in Table 3 in this Example 2, and the CPU running time is 110.688 sec. when $\frac{2\mathscr{Y}}{3}$, and 117.578 when $\eta(\mathscr{Y}) = \frac{\mathscr{Y}^3}{3}$. Figure 3 represents the AEs of Example 2 when $\nu_1 = 8$, $\eta(\mathscr{Y}) = \frac{2\mathscr{Y}}{3}$ and $\eta(\mathscr{Y}) = \frac{\mathscr{Y}^3}{3}$ respectively. Figure 4 compare the exact and approximate solutions when $\nu_2 = 8$ and $\eta(\mathscr{Y}) = \frac{2\mathscr{Y}}{3}$ and $\eta(\mathscr{Y}) = \frac{\mathscr{Y}^3}{3}$ respectively. The results show that, even by a few points, our technique is more accurate.

Table 3. The *AEs* of Example 2 with virous of $\mathscr{Y}$ and $\eta(\mathscr{Y})$ at $\nu_2 = 8$

$\mathscr{Y}$	$\nu_2 = 8,\ \eta(\mathscr{Y}) = \frac{2\mathscr{Y}}{3}$	$\nu_2 = 8,\ \eta(\mathscr{Y}) = \frac{\mathscr{Y}^3}{3}$
0	6.9389×10^{-18}	7.3726×10^{-18}
0.1	3.6863×10^{-18}	1.5179×10^{-18}
0.2	1.9949×10^{-17}	4.7705×10^{-18}
0.3	2.1684×10^{-18}	1.1601×10^{-17}
0.4	4.4235×10^{-17}	7.2642×10^{-18}
0.5	7.5894×10^{-17}	3.0358×10^{-18}
0.6	1.4268×10^{-16}	4.0549×10^{-17}
0.7	2.7181×10^{-16}	3.9397×10^{-17}
0.8	4.3715×10^{-16}	2.7539×10^{-17}
0.9	7.2381×10^{-16}	7.0690×10^{-17}
1.0	2.4173×10^{-15}	1.3965×10^{-16}

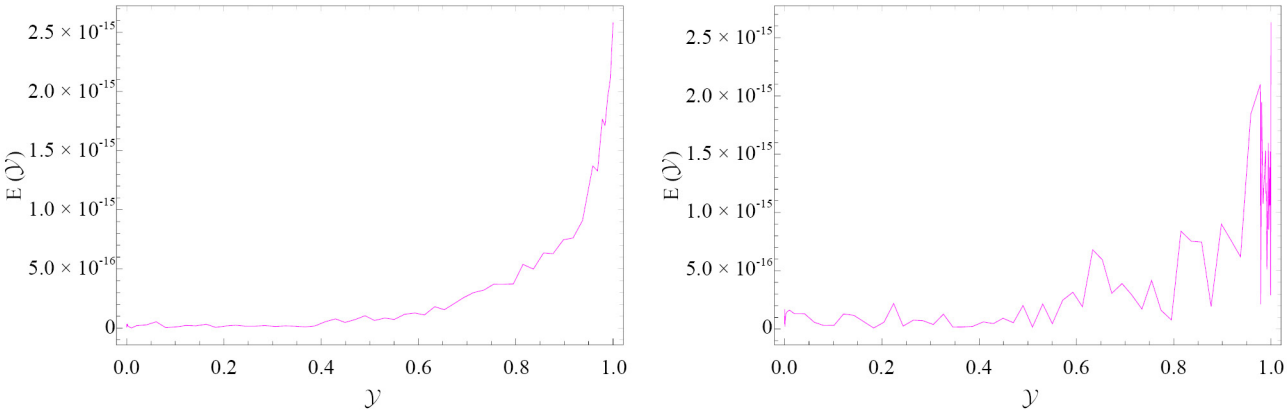

Figure 3. The AEs for Example 2 when $\nu_1 = 8$, $\eta(\mathscr{Y}) = \frac{2\mathscr{Y}}{3}$ and $\eta(\mathscr{Y}) = \frac{\mathscr{Y}^3}{3}$ respectively

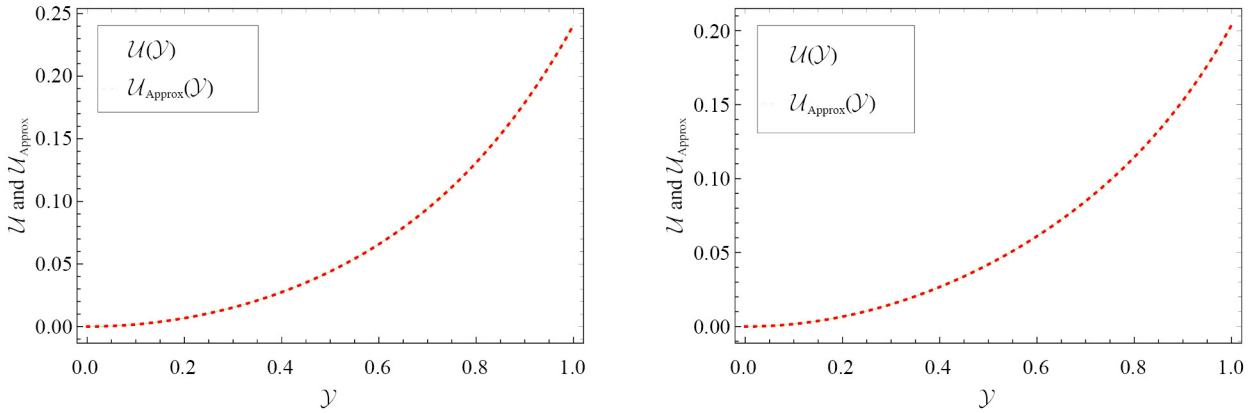

Figure 4. The $\hat{\mathscr{U}}_{Approx}(\mathscr{Y})$ and $\hat{\mathscr{U}}(\mathscr{Y})$ for Example 2 when $\nu_2 = 8$ and $\nu_1 = 8$, $\eta(\mathscr{Y}) = \frac{2\mathscr{Y}}{3}$ and $\eta(\mathscr{Y}) = \frac{\mathscr{Y}^3}{3}$ respectively

Taking $\nu_2 = 8$ and $\eta(\mathscr{Y}) = \frac{2\mathscr{Y}}{3}$, we acquire the numerical outcomes $\hat{\mathscr{U}}_{Approx}(\mathscr{Y})$ of Example 2 as:

$$\begin{aligned}\hat{\mathscr{U}}_{Approx}(\mathscr{Y}) =& 0. + 0.333333\mathscr{Y} + 3.4639 \times 10^{-14}\mathscr{Y}^2 - 3.63654 \times 10^{-13}\mathscr{Y}^3 + 1.75115 \times 10^{-12}\mathscr{Y}^4 \\ &+ 0.148148\mathscr{Y}^5 + 6.03867 \times 10^{-12}\mathscr{Y}^6 - 4.24364 \times 10^{-12}\mathscr{Y}^7 + 1.20029 \times 10^{-12}\mathscr{Y}^8\end{aligned} \tag{31}$$

Taking $\nu_2 = 8$ and $\eta(\mathscr{Y}) = \frac{\mathscr{Y}^3}{3}$, we acquire the numerical outcomes $\hat{\mathscr{U}}_{Approx}(\mathscr{Y})$ of Example 2 as:

$$\begin{aligned}\hat{\mathscr{U}}_{Approx}(\mathscr{Y}) =& 0. + 1.94289 \times 10^{-16}\mathscr{Y} + 0.166667\mathscr{Y}^2 + 4.65183 \times 10^{-14}\mathscr{Y}^3 - 2.14551 \times 10^{-13}\mathscr{Y}^4 \\ &+ 5.25247 \times 10^{-13}\mathscr{Y}^5 - 6.92196 \times 10^{-13}\mathscr{Y}^6 + 0.037037\mathscr{Y}^7 - 1.23628 \times 10^{-13}\mathscr{Y}^8.\end{aligned} \tag{32}$$

Example 3 We consider the non-linear linear VOC-ψ-FRDE:

$$\begin{cases} {}^{c}D_{\mathscr{Y}}^{\eta(\mathscr{Y}),\,\psi}\hat{\mathscr{U}}(\mathscr{Y}) + (\hat{\mathscr{U}}(\mathscr{Y}))^2 = G(\mathscr{Y}), \\ \\ \mathscr{Y}(0) = 0, \end{cases} \tag{33}$$

$G(\mathscr{Y})$ is given from the exact solution $\hat{\mathscr{U}}(\mathscr{Y}) = \mathscr{Y}\sin(\mathscr{Y})$, $\psi(\mathscr{Y}) = \frac{\mathscr{Y}^4}{5}$, and $\eta(\mathscr{Y}) = \mathscr{Y}\sin(\mathscr{Y})$, where ${}^{c}D_{\mathscr{Y}}^{\eta(\mathscr{Y}),\,\psi}\hat{\mathscr{U}}(\mathscr{Y})$ is VOC-ψ-FRDE.

We obtain L_∞ with various values of ν_2 in Table 4 in this Example 3. Figure 5 illustrates the AEs of Example 3 when $\eta(\mathscr{Y}) = \mathscr{Y}sin(\mathscr{Y})$, $\psi(\mathscr{Y}) = \frac{\mathscr{Y}^4}{5}$, $\nu_1 = 10$, and $\nu_1 = 12$, respectively. Figure 6 compare the exact and approximate solutions when $\eta(\mathscr{Y}) = \mathscr{Y}sin(\mathscr{Y})$, $\psi(\mathscr{Y}) = \frac{\mathscr{Y}^4}{5}$, $\nu_1 = 10$, and $\nu_1 = 12$, respectively. The convergence decay of our method is illustrated in Figure 7. The findings demonstrate that our method provides improved accuracy even with a small number of data points.

Table 4. The *MAE* of Example 3 with virous of ν_2, $\eta(\mathscr{Y}) = \mathscr{Y}\sin(\mathscr{Y})$, and $\psi(\mathscr{Y}) = \frac{\mathscr{Y}^4}{5}$

$\eta(\mathscr{Y})$	$\nu_2 = 2$	$\nu_2 = 4$	$\nu_2 = 6$	$\nu_2 = 8$	$\nu_2 = 10$	$\nu_2 = 12$
$\mathscr{Y}sin(\mathscr{Y})$	3.03×10^{-2}	1.3×10^{-4}	2.3×10^{-7}	2.4×10^{-10}	1.6×10^{-13}	3.3×10^{-16}
CPU (Sec.)	22.093	65.499	118.658	259.327	358.594	512.453

Taking $\nu_2 = 10$ and $\eta(\mathscr{Y}) = \mathscr{Y}\sin(\mathscr{Y})$, we acquire the numerical outcome $\hat{\mathscr{U}}_{Approx}(\mathscr{Y})$ of Example 3 as:

$$\begin{aligned}\hat{\mathscr{U}}_{Approx}(\mathscr{Y}) =& 0. + 9.94116 \times 10^{-12}\mathscr{Y} + 1.\mathscr{Y}^2 + 9.55438 \times 10^{-9}\mathscr{Y}^3 - 0.166667\mathscr{Y}^4 + 3.802 \times 10^{-7}\mathscr{Y}^5 \\ &+ 0.00833224\mathscr{Y}^6 + 1.95037 \times 10^{-6}\mathscr{Y}^7 - 0.000200587\mathscr{Y}^8 + 1.42051 \times 10^{-6}\mathscr{Y}^9 \\ &+ 2.31427 \times 10^{-6}\mathscr{Y}^{10}.\end{aligned} \tag{34}$$

Taking $\nu_2 = 12$ and $\eta(\mathscr{Y}) = \mathscr{Y}\sin(\mathscr{Y})$, we acquire the numerical outcome $\hat{\mathscr{U}}_{Approx}(\mathscr{Y})$ of Example 3 as:

$$\begin{aligned}\hat{\mathscr{U}}_{Approx}(\mathscr{Y}) = &-5.55112\times10^{-17} - 5.9952\times10^{-15}\mathscr{Y} + 1.\mathscr{Y}^2 - 1.16415\times10^{-11}\mathscr{Y}^3 - 0.166667\mathscr{Y}^4 \\ &- 1.0153\times10^{-9}\mathscr{Y}^5 + 0.00833334\mathscr{Y}^6 - 1.29898\times10^{-8}\mathscr{Y}^7 - 0.000198387\mathscr{Y}^8 \\ &+ -3.31785\times10^{-8}\mathscr{Y}^9 2.78426\times10^{-6}\mathscr{Y}^{10} - 1.49622\times10^{-8}\mathscr{Y}^{11} - 2.12011\times10^{-8}\mathscr{Y}^{12}.\end{aligned} \tag{35}$$

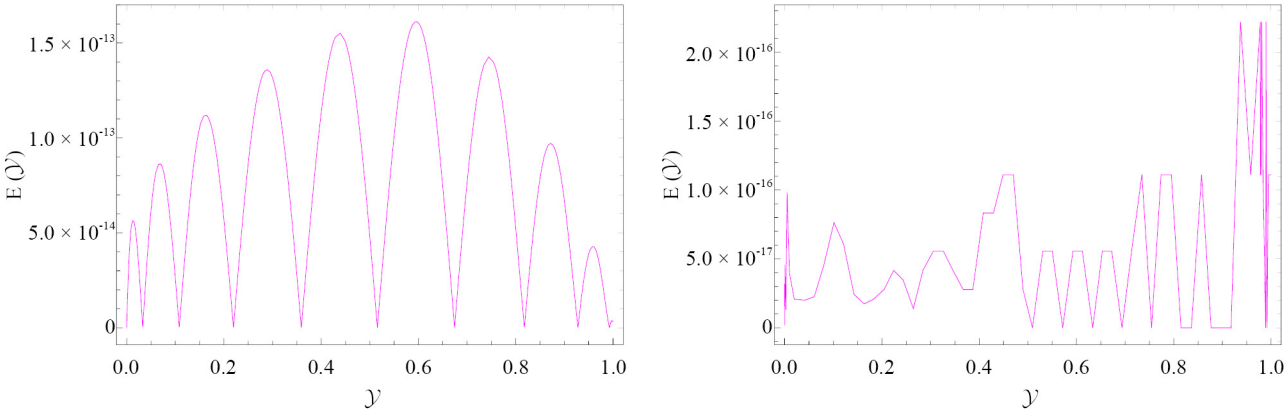

Figure 5. The AEs for Example 3 when $\eta(\mathscr{Y}) = \mathscr{Y}sin(\mathscr{Y})$, $\psi(\mathscr{Y}) = \frac{\mathscr{Y}^4}{5}$, $\nu_1 = 10$, and $\nu_1 = 12$, respectively

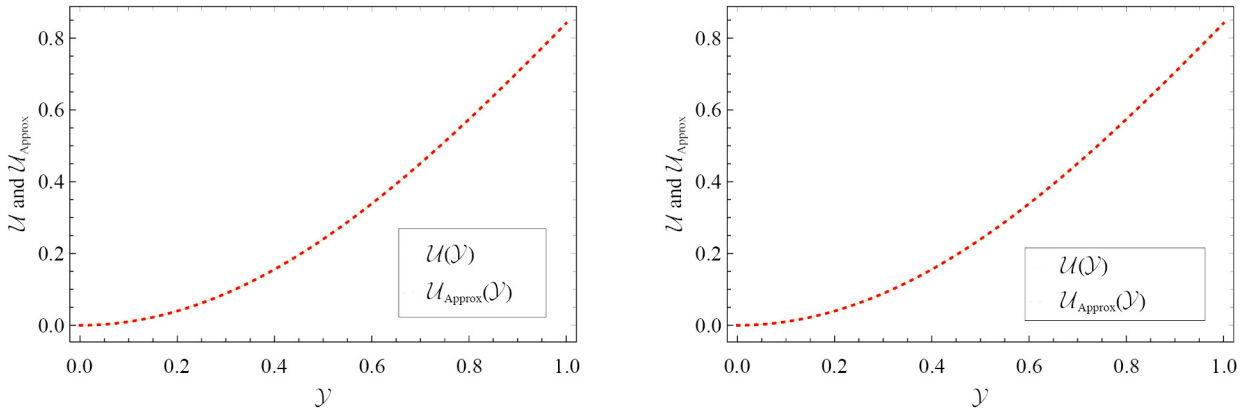

Figure 6. The $\hat{\mathscr{U}}_{Approx}(\mathscr{Y})$ and $\hat{\mathscr{U}}(\mathscr{Y})$ for Example 3 when $\eta(\mathscr{Y}) = \mathscr{Y}sin(\mathscr{Y})$, $\psi(\mathscr{Y}) = \frac{\mathscr{Y}^4}{5}$, $\nu_1 = 10$, and $\nu_1 = 12$, respectively

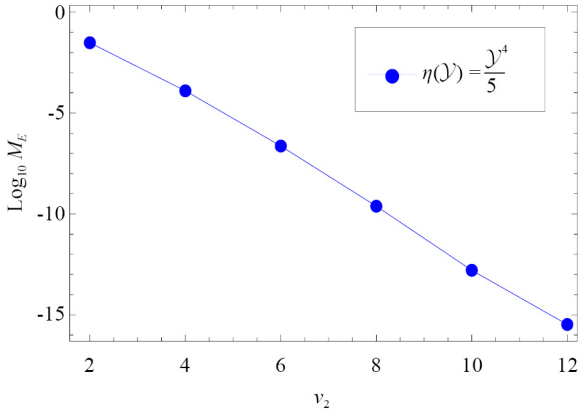

Figure 7. The M_E convergence for Example 3 when $\eta(\mathscr{Y}) = \mathscr{Y} sin(\mathscr{Y})$ and $\psi(\mathscr{Y}) = \frac{\mathscr{Y}^4}{5}$

5. Conclusion

Our primary objective is to improve spectral algorithms for solving non-linear VOC-ψ-FRDE using the SL-GL-C method, and Caputo-ψ fractional differential equation. These new algorithms are developed by transforming the mentioned problems into a system of algebraic equations. We have included numerical examples that demonstrate for assessing the accuracy and practicality of the current algorithms. The comparisons provided show the accuracy and effectiveness of the spectral collection method. Examples that demonstrate a concept or principle. Beyond solving fractional Riccati-type models, the proposed spectral collocation method shows strong potential for control and synchronization of nonlinear systems. Its exponential convergence enables more accurate reference trajectories and state estimates, enhancing adaptive fuzzy, backstepping, and neural control schemes. It also improves modeling of uncertain systems with input nonlinearities and nonlinear optimal control tasks, such as gas compressors, while capturing fractional-order effects in flexible robot manipulators. These features highlight its promise for advancing fractional-order modeling in practical control and synchronization applications.

Acknowledgement

This work was supported by Princess Nourah bint Abdulrahman University Researchers Supporting Project number (PNURSP2024R157), Princess Nourah bint Abdulrahman University, Riyadh, Saudi Arabia. The authors are thankful to the Deanship of Graduate Studies and Scientific Research at University of Bisha for supporting this work through the Fast-Track Research Support Program. This work of the last author (AB) was supported by Grambling State University as the Endowed Chair of Mathematics. The author thankfully acknowledges this support.

Conflict of interest

The authors declare no competing financial interest.

References

[1] Doha EH, Bhrawy AH, Abdelkawy MA, Hafez RM. A Jacobi collocation approximation for nonlinear coupled viscous Burgers' equation. *Central European Journal of Physics*. 2014; 12: 111–122.

[2] Bhrawy AH, Abdelkawy MA, Alzahrani AA, Baleanu D, Alzahrani EO. A chebyshev-laguerre-gauss-radau collocation scheme for solving a time fractional sub-diffusion equation on a semi-infinite domain. *Romanian Reports in Physics*. 2015; 6(4): 490–498.

[3] Amin AZ, Abdelkawy MA, Hashim I. A space-time spectral approximation for solving nonlinear variable-order fractional convection-diffusion equations with nonsmooth solutions. *International Journal of Modern Physics C*. 2023; 34(3): 2350041.

[4] Metzler R, Klafter J. The random walk's guide to anomalous diffusion: a fractional dynamics approach. *Physics Reports*. 2000; 339(1): 1–77.

[5] Bhrawy AH, Alhuthali MS, Abdelkawy MA. New solutions for (1 + 1)-dimensional and (2 + 1)-dimensional Ito equations. *Mathematical Problems in Engineering*. 2012; 2012: 1–4.

[6] Azar AT, Radwan AG, Vaidyanathan S. *Fractional Order Systems: Optimization, Control, Circuit Realizations and Applications*. Academic Press; 2018.

[7] Kilbas AA, Srivastava HM, Trujillo JJ. *Theory and Applications of Fractional Differential Equations*. Vol. 204. Elsevier; 2006.

[8] Mantegna RN, Stanley HE. *Introduction to Econophysics: Correlations and Complexity in Finance*. Cambridge University Press; 1999.

[9] Skovranek T, Despotovic V. Signal prediction using fractional derivative models. In: *Handbook of Fractional Calculus with Applications: Applications in Engineering, Life and Social Sciences, Part B*. Berlin, Boston: De Gruyter; 2019. p.179–206.

[10] Rabiei K, Razzaghi M. Fractional-order Boubaker wavelets method for solving fractional Riccati differential equations. *Applied Numerical Mathematics*. 2021; 168: 221–234.

[11] Yuttanan B, Razzaghi M, Vo TN. Fractional-order generalized Legendre wavelets and their applications to fractional Riccati differential equations. *International Journal of Nonlinear Sciences and Numerical Simulation*. 2023; 24(1): 57–69.

[12] Doha EH, Abdelkawy M, Baleanu D. Approximate solutions for solving nonlinear variable-order fractional Riccati differential equations. *Nonlinear Analysis: Modelling and Control*. 2019; 24(2): 176–188.

[13] Momani S, Djeddi N, Al-Smadi M, Al-Omari S. Numerical investigation for Caputo-Fabrizio fractional Riccati and Bernoulli equations using iterative reproducing kernel method. *Applied Numerical Mathematics*. 2021; 170: 418–434.

[14] Tvyordyj DA. Hereditary Riccati equation with fractional derivative of variable order. *Journal of Mathematical Sciences*. 2021; 253: 564–572.

[15] Nikan O, Rashidinia J, Jafari H. Numerically pricing American and European options using a time fractional Black–Scholes model in financial decision-making. *Alexandria Engineering Journal*. 2025; 112: 235–245.

[16] Luo M, Qiu W, Nikan O, Avazzadeh Z. Second-order accurate, robust and efficient ADI Galerkin technique for the three-dimensional nonlocal heat model arising in viscoelasticity. *Applied Mathematics and Computation*. 2023; 440: 127655.

[17] Qiu W, Nikan O, Avazzadeh Z. Numerical investigation of generalized tempered-type integrodifferential equations with respect to another function. *Fractional Calculus and Applied Analysis*. 2023; 26(6): 2580–2601.

[18] Ali A, Minamoto T. A new numerical technique for solving ψ-fractional Riccati differential equations. *Journal of Applied Analysis and Computation*. 2023; 13(2): 1027–1043.

[19] Almeida R. On the variable-order fractional derivatives with respect to another function. *Mathematical Equations*. 2025; 99(2): 805–822.

[20] Ben Brahim H, El Alaoui FZ, Tajani A, Torres DFM. Existence and uniqueness of mild solutions for a class of psi-Caputo time-fractional systems of order from one to two. *Fractional Calculus and Applied Analysis*. 2025; 28: 2357–2394. Available from: https://doi.org/10.1007/s13540-025-00434-0.

[21] Ali A, Minamoto T, Shah R, Nonlaopon K. A novel numerical method for solution of fractional partial differential equations involving the Ψ-Caputo fractional derivative. *AIMS Mathematics*. 2023; 8(1): 2137–2153.

[22] Zhao T, Zhao Z, Li C, Li D. Spectral approximation of ψ-fractional differential equation based on mapped Jacobi functions. *arXiv:231216426*. 2023.

[23] Boulkroune A, Zouari F, Boubellouta A. Adaptive fuzzy control for practical fixed-time synchronization of fractional-order chaotic systems. *Journal of Vibration and Control*. 2025; 10775463251320258.

[24] Boulkroune A, Hamel S, Zouari F, Boukabou A, Ibeas A. Output-feedback controller based projective lag-synchronization of uncertain chaotic systems in the presence of input nonlinearities. *Mathematical Problems in Engineering*. 2017; 2017(1): 8045803.

[25] Zouari F, Saad KB, Benrejeb M. Robust neural adaptive control for a class of uncertain nonlinear complex dynamical multivariable systems. *International Review of Modelling and Simulation*. 2012; 5(5): 2075–2103.

[26] Zouari F, Saad KB, Benrejeb M. Adaptive backstepping control for a class of uncertain single input single output nonlinear systems. In: *10th International Multi-Conferences on Systems, Signals & Devices (SSD13)*. IEEE; 2013. p.1–6.

[27] Delzanno GL. Multi-dimensional, fully-implicit, spectral method for the Vlasov–Maxwell equations with exact conservation laws in discrete form. *Journal of Computational Physics*. 2015; 301: 338–356.

[28] Chen Y, Zhou J. Error estimates of spectral Legendre–Galerkin methods for the fourth-order equation in one dimension. *Applied Mathematics and Computation*. 2015; 268: 1217–1226.

[29] Abdelkawy MA, Amin AZM, Lopes AM. Fractional-order shifted Legendre collocation method for solving non-linear variable-order fractional Fredholm integro-differential equations. *Computational and Applied Mathematics*. 2022; 41(1): 1–21.

[30] Amin AZ, Abdelkawy MA, Solouma E, Al-Dayel I. A spectral collocation method for solving the non-linear distributed-order fractional Bagley–Torvik differential equation. *Fractal and Fractional*. 2023; 7(11): 780.

[31] Abd-Elhameed WM, Youssri YH. New formulas of the high-order derivatives of fifth-kind Chebyshev polynomials: Spectral solution of the convection–diffusion equation. *Numerical Methods for Partial Differential Equations*. 2024; 40(2): e22756.

[32] Amin AZ, Lopes AM, Hashim I. A space-time spectral collocation method for solving the variable-order fractional Fokker–Planck equation. *Journal of Applied Analysis and Computation*. 2023; 13: 969–985.

[33] Amin A, Abdelkawy M, Amin A, Lopes AM, Alluhaybi A, Hashim I. Legendre–Gauss–Lobatto collocation method for solving multi-dimensional systems of mixed Volterra–Fredholm integral equations. *AIMS Mathematics*. 2023; 8: 20871–20891.

[34] Tedjani AH, Amin AZ, Abdel-Aty AH, Abdelkawy MA, Mahmoud M. Legendre spectral collocation method for solving nonlinear fractional Fredholm integro-differential equations with convergence analysis. *AIMS Mathematics*. 2024; 9(4): 7973–8000.

[35] Magdy E, Abd-Elhameed WM, Youssri YH, Moatimid GM, Atta AG. A potent collocation approach based on shifted Gegenbauer polynomials for nonlinear time fractional Burgers' equations. *Contemporary Mathematics*. 2023: 647–665.

[36] Amin AZ, Abdelkawy MA, Soluma EM, Babatin MM. A space-time spectral approximation for solving two dimensional variable-order fractional convection-diffusion equations with nonsmooth solutions. *International Journal of Modern Physics C*. 2024; 35(7): 2450088.

[37] Ezz-Eldien SS. On solving systems of multi-pantograph equations via spectral tau method. *Applied Mathematics and Computation*. 2018; 321: 63–73.

[38] Doha EH, Abdelkawy MA, Amin AZM, Baleanu D. Shifted Jacobi spectral collocation method with convergence analysis for solving integro-differential equations and system of integro-differential equations. *Nonlinear Analysis: Modelling and Control*. 2019; 24(3): 332–352.

[39] Ahmed HM, Hafez RM, Abd-Elhameed WM. A computational strategy for nonlinear time-fractional generalized Kawahara equation using new eighth-kind Chebyshev operational matrices. *Physica Scripta*. 2024; 99(4): 045250.

[40] Abdelkawy MA, Taha TM. An operational matrix of fractional derivatives of Laguerre polynomials. *Walailak Journal of Science and Technology*. 2014; 11(12): 1041–1055.

[41] Youssri YH, Abd-Elhameed WM. Numerical spectral Legendre–Galerkin algorithm for solving time fractional telegraph equation. *Romanian Journal of Physics*. 2018; 63(107): 1–16.

[42] Bhrawy AH, Abdelkawy MA, Mallawi F. An accurate Chebyshev pseudospectral scheme for multi-dimensional parabolic problems with time delays. *Boundary Value Problems*. 2015; 2015(1): 103.

[43] Doha EH, Abd-Elhameed WM. Efficient spectral ultraspherical-dual-Petrov–Galerkin algorithms for the direct solution of $(2n + 1)$th-order linear differential equations. *Mathematics and Computers in Simulation*. 2009; 79(11): 3221–3242.

[44] Doha EH, Abd-Elhameed WM, Youssri YH. Efficient spectral-Petrov–Galerkin methods for the integrated forms of third- and fifth-order elliptic differential equations using general parameters generalized Jacobi polynomials. *Computational and Applied Mathematics*. 2012; 218(15): 7727–7740.

[45] Fahad HM, Fernandez A, Rehman MU, Siddiqi M. Tempered and Hadamard-type fractional calculus with respect to functions. *Mediterranean Journal of Mathematics*. 2021; 18(4): 143.

[46] Fan E, Li C, Li Z. Numerical approaches to Caputo–Hadamard fractional derivatives with applications to long-term integration of fractional differential systems. *Communications in Nonlinear Science and Numerical Simulation*. 2022; 106: 106096.

[47] Li C, Li Z. Stability and logarithmic decay of the solution to Hadamard-type fractional differential equation. *Journal of Nonlinear Science*. 2021; 31: 1–60.

[48] Li C, Li Z, Wang Z. Mathematical analysis and the local discontinuous Galerkin method for Caputo–Hadamard fractional partial differential equation. *Journal of Scientific Computing*. 2020; 85: 1–27.

[49] Li C, Li Z. On blow-up for a time–space fractional partial differential equation with exponential kernel in temporal derivative. *Journal of Mathematical Sciences*. 2022; 266(3): 381–394.

[50] Almeida R, Malinowska AB, Monteiro MTT. Fractional differential equations with a Caputo derivative with respect to a kernel function and their applications. *Mathematical Methods in the Applied Sciences*. 2018; 41(1): 336–352.

[51] Almeida R. Variational problems of variable fractional order involving arbitrary kernels. *AIMS Mathematics*. 2022; 7(10): 18690–18707.

[52] Almeida R. A numerical scheme for a generalized fractional derivative with variable order. In: *International Conference on the Dynamics of Information Systems*. Springer; 2023. p.20–30.

[53] Canuto C, Hussaini MY, Quarteroni A, Zang TA. *Spectral Methods: Fundamentals in Single Domains*. Springer Science & Business Media; 2007.

[54] Amin AZ, Lopes AM, Hashim I. A Chebyshev collocation method for solving the non-linear variable-order fractional Bagley–Torvik differential equation. *International Journal of Nonlinear Sciences and Numerical Simulation*. 2022; 24(5): 1613–1630.